RSS Technical Report 102210 **October 22, 2010**

The Version-6 Calibration of SSM/I

By: Frank J. Wentz

Remote Sensing Systems, Santa Rosa, CA

Prepared By:

Remote Sensing Systems

444 Tenth Street, Suite 200, Santa Rosa, CA 95401 (707) 545-2904

Table of Contents

1. Introduction

The Special Sensor Microwave Imagers (SSM/I) are a series of 6 satellite radiometers that have been in operation since 1987. These satellite sensors measure the natural microwave emission coming from the Earth's surface in the spectral band from 19 to 85 GHz. These emission measurements contain valuable information on many important climate variables including winds over the ocean, the moisture and rain in the atmosphere, sea ice, and snow cover. However, the extraction of this information from the raw satellite measurements is a complicated process requiring considerable care and diligence. The first step in the process is the generation of Fundamental Climate Data Records (FCDR) of the sensor measurements in term of antenna temperatures (T_A) and brightness temperatures (T_B). It is absolutely essential that proper satellite inter-calibration methods be employed when producing these SSM/I FCDRs.

Since the first SSM/I was launched in 1987, Remote Sensing Systems (RSS) has been providing SSM/I data to the research and climate communities. The most current RSS dataset is called Version 6 and is generally recognized as the most complete and accurate SSM/I FCDR available. The V6 T_A and T_B are currently being used at about 20 institutions worldwide. This document describes the calibration procedure that is used to convert the raw SSM/I sensor counts that are sent down from the spacecraft to fully calibrated T_A and T_B.

This document assumes the reader in familiar with the SSM/I from both a hardware standpoint and an analysis standpoint. The following references provide ample information in these two areas: *Hollinger et al*. 1987; *Wentz* 1988, 1991, 1993, 1997; *Colton and Poe*, 1999; *Hilburn and Wentz*, 2008.

2. Unadjusted Antenna Temperature

In computing the unadjusted SSM/I antenna temperature (T_A), the basic assumption is that the radiometer output voltage in linearly related to the input power at the mixer/preamplifier. Nonlinear effects such as imperfections in the square-law detector and the IF amplifier compression are assumed to negligible. Under these assumptions, the T_A is given by [*Wentz*, 1991]

$$T_A = \frac{(T_{Ah} - T_{Ac})C + T_{Ac}C_h - T_{Ah}C_c}{C_h - C_c} \tag{1}$$

The terms C_c, C_h, and C are the radiometer counts (i.e., output voltage) when the radiometer is looking at the cold calibration target, the hot calibration target, and the earth scene, respectively. The temperatures T_{Ac} and T_{Ah} are the effective temperatures of the cold and hot calibration targets. Equation (1) is simply expressing the assumption that the radiometer counts vary linearly as the scene temperature varies from T_{Ac} to T_{Ah}.

One difficulty is accurately specifying T_{Ac} and T_{Ah}. For example, the cold target is a mirror pointing towards cold space, which has a temperature of 2.73 K. However, if the mirror is not a perfect reflector or if the cold measurement is receiving radiation from other sources (i.e., spillover effects), the true value for T_{Ac} will be greater than 2.73K. The specification of T_{Ah} is even more difficult. In this case, one must infer T_{Ah} from thermistor readings attached to the hot target. The thermistors are embedded into the hot load, and there will be some error in using these readings to estimate the effective surface temperature of the hot load. Thermal gradients over the extent of the hot load will also cause problems (SSM/I has only 3 thermistors).

In computing the unadjusted T_A, we use a relatively simple model for T_{Ac} and T_{Ah}. The cold temperature is assumed to be 2.7 K for the 19, 22, and 37 GHz channels. For the 85 GHz channels, a value of 3.2 K is assumed. At 85 GHz, the Rayleigh-Jeans approximation to the Planck equation begins to break down. A common technique for handling this problem is to use a somewhat larger value for T_{Ac} to compensate for the slight non-linearity between spectral radiance and brightness temperature that occurs at the higher microwave frequencies. Accordingly we use a value of T_{Ac}=3.2K at 85 GHz.

For the hot load temperature, we use the following

$$T_{Ah} = \overline{T}_h + \xi\left(T_p - \overline{T}_h\right) \tag{2}$$

The temperature $\overline{T}_h$ is the average of the 3 thermistor readings and the temperature T_p is the reading from the single thermistor on the SSM/I drum plate facing the hot load. The coefficient ξ is a value derived from prelaunch thermal-vacuum measurements and its value is 0.01 [*Hollinger et al.*, 1987]. For the F13 SSM/I, only hot-load thermistor 2 is used for $\overline{T}_h$ because the other 2 thermistors displayed considerable noise [*Colton and Poe*, 1999].

Noise in C_c and C_h is reduced by averaging measurements from adjacent scans. We use a time window of ±12 seconds centered on the scan being processed. If there are no data gaps, this time window will include 7 A/B scan pairs. For the 19-37 GHz channels, calibration counts are only collected during the A scan. For 85 GHz, calibration counts are collected for both the A and B scans. For each scan, 5 calibration measurements are taken of the cold target and another 5 for the hot target. Thus our ±12 seconds time window provides 35 cold counts and 35 hot count for each of the lower-frequency channels. At 85 GHz, there are twice as many count values. This is a sufficient number of samples to reduce the noise in the calibration counts to an acceptable level. In equation (1), C_c and C_h represent average values over 7 scans. The same type of scan averaging is also done for the hot load thermistor readings, but this has little effect.

3. Along-Scan Correction

One of the first SSM/I calibration problems that was detected was an along-scan error [*Wentz*, 1991]. Towards the end of the Earth scan, the cold calibration mirror began to intrude into the field of view of the feedhorn. As a result, the T_A measurements exhibit a systematic roll-off of about 1K at the end of the scan.

To find a correction for the along-scan error, the first step is to remove variations due to changing incidence angle and wind direction. If not accounted for, these two effects can introduce spurious signals into the derivation of the along-scan correction. The adjusted T_A, denoted by a single prime, is given by

$$T'_{Aij} = T_{Aij} - \frac{\partial T_A}{\partial \theta_{eia}}\left(\theta_{eia} - 53.25^o\right) - f_{rtm}\left(\phi_r\right) \tag{3}$$

where we have now introduced the subscripts *i* and *j* to denote the channel number and satellite number, respectively. The channel number goes from *i*=1 to 7 and corresponds to 19V, 19H,

22V, 37V, 37H, 85V, and 85H, respectively. The satellite number goes from j=1 to 6 and corresponds to F08, F10, F11, F13, F14, and F15, respectively. These subscripts have this same definition through this document. The term T_{Aij} is the unadjusted T_A discussed in Section 2.

The first term in (3) is intended to normalize the antenna temperatures to a constant incidence angle for 53.25°. The derivative of T_A w.r.t. the Earth incidence angle θ_{eai} is estimated from the T_A values. The v-pol derivative is fairly invariant for ocean, rain-free scenes, having a typical value of +2 K/deg. The h-pol derivative is more sensitive to the variation in atmospheric absorption due to water vapor and clouds, and its values can typically range from -1 K/deg for clear dry scenes to +1 K/deg for cloudy wet scenes. The v-pol minus h-pol difference exhibited by the T_As at the various frequencies is a good indicator of the atmospheric absorption, and a relative simply algorithm can be used to estimate $\partial T_A / \partial \theta_{eia}$. The second term in (3) corrects for wind direction effects. The argument ϕ_r is the relative angle between the wind direction and the SSM/I azimuth look direction. NCEP values for wind speed and direction along with the azimuth angle of the SSM/I observation are used to compute the change in antenna temperature just due to wind direction [*Wentz*, 1992]. This component is then subtracted from T_A. The adjustments for incidence angle and wind direction are only done for ocean observations. The resulting T'_{Aij} is then the isotropic (no wind direction effects) T_A at an Earth incidence angle of 53.25°.

Our model for the along-scan error is

$$T'_{Aij} = \left(1 - \Psi_{ij}(\omega)\right) T''_{Aij} + \Psi_{ij}(\omega) T_{Ac} \tag{4}$$

where the observed T_A on the left-hand side is the weighted sum of the T_A coming from the Earth T''_{Aij} and the T_A coming from the cold mirror T_{Ac}, which we assume to be 2.7 K for the lower frequency channels and 3.2 for 85 GHz, as discussed above. The weight factor $\Psi_{ij}(\omega)$ is a function of the scan angle ω, which represents 64 scan positions for the 19 through 37 GHz channels and 128 scan positions for the 85 GHz channels. The T_A corrected for along-scan errors is then given by inverting (4).

$$T''_{Aij} = \frac{T'_{Aij} - \Psi_{ij}(\omega) T_{Ac}}{1 - \Psi_{ij}(\omega)} \tag{5}$$

The derivation of $\Psi_{ij}(\omega)$ is essentially an averaging process. T'_{Aij} values for ocean, rain-free observations are averaged into cell position bins (i.e. ω-bins) and into 10^o latitude zones from 50S to 50N. If we did not use latitude zones and simply averaged all observations into ω-bins, then the average latitude for the ω-bins would vary considerably across the scan. For example, the SSM/I right-most cell is also the north-most cell as the satellite approaches the poles. The ω-bin for this cell will have a higher average latitude than the left-most cell. Since all the SSM/I channels are sensitive to water vapor and since water vapor has a strong latitudinal variation, spurious features would occur due to non-uniform latitude sampling. By pre-averaging into 10^o latitude bins, this effect is greatly mitigated. We experimented with other methods to find the along-scan correction such as making 1^o latitude/longitude T_A maps, calculating the change in T_A with latitude, and then making a correction. This method gave essentially the same results, but was more complicated. Using the 10^o pre-averaging method is sufficient.

All available observations are used to find the (ω, latitude)-bin averages. For example for F13, which has the longest operational period, 10 years of observations are averaged. These averages are denote by $\langle T'_{Aij} \rangle_{\omega,lat}$. The pre-averages are then averaged over the 10 zones as follows:

$$\langle T'_{Aij} \rangle_{\omega} = \frac{\sum_{lat=1}^{10} n_{lat} \langle T'_{Aij} \rangle_{\omega,lat}}{\sum_{lat=1}^{10} n_{lat}} \tag{6a}$$

$$\langle T'_{Aij} \rangle = \frac{\sum_{\omega} \sum_{lat=1}^{10} n_{lat} \langle T'_{Aij} \rangle_{\omega,lat}}{\sum_{\omega} \sum_{lat=1}^{10} n_{lat}} \tag{6b}$$

Equation (6a) represents a properly averaged T_A binned according to just scan angle, and (6b) is T_A properly averaged over the entire scan. We define the scan correction $\Psi_{ij}(\omega)$ such that its average over ω is zero, and hence according to equation (4) the scan-average T_A is T''_{Aij}, which is the same as $\langle T'_{Aij} \rangle$ equation (6b), i.e., $T''_{Aij} \leftarrow \langle T'_{Aij} \rangle$. The ω-bin average for the uncorrected T_A is T'_{Aij} in equation (4) and $\langle T'_{Aij} \rangle_{\omega}$ in equation (6a), i.e., $T'_{Aij} \leftarrow \langle T'_{Aij} \rangle_{\omega}$. Then, inverting (4) to yield $\Psi_{ij}(\omega)$ and applying the two substitutions just given results in

$$\Psi_{ij}(\omega) = \frac{\left\langle T'_{Aij} \right\rangle - \left\langle T'_{Aij} \right\rangle_{\omega}}{\left\langle T'_{Aij} \right\rangle - T_{Ac}} \tag{7}$$

In this way, tables are made for each satellite *j* and each channel *i* that gives $\Psi_{ij}(\omega)$ for the 64 cell positions for the lower frequencies and for the 128 cell positions for the higher frequencies. Figure 1 show $\Psi_{ij}(\omega)$ for all satellites and all channels. The color coding used to display the 7 different channels is given in Table 1 below. Table 1 also gives the color coding for figures to be presented later in which the colors denote the 6 different SSM/I.

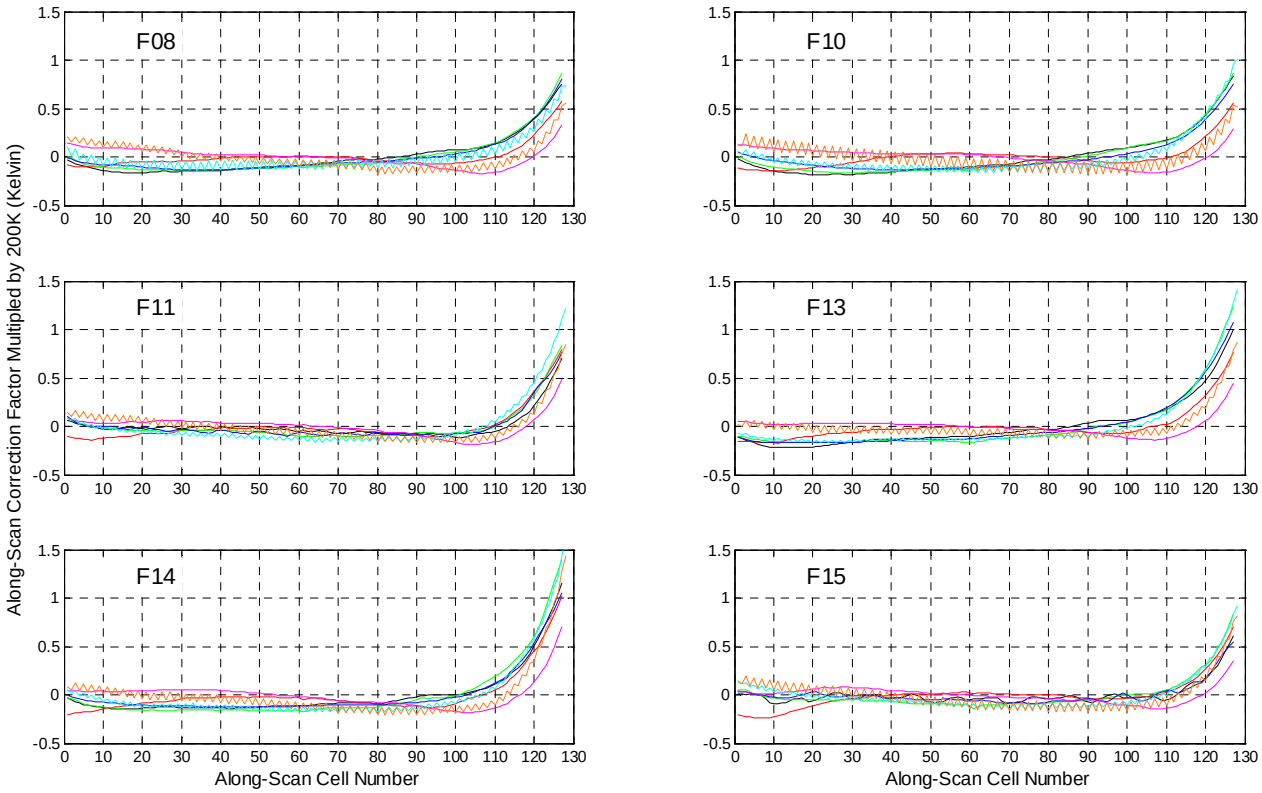

Figure 1. The along-scan correction that is applied to the SSM/I T_A. To show these results in terms of a value indicative of the T_A adjustment, $\Psi_{ij}(\omega)$ has been multiplied by 200K. The adjustment has the effect of increasing T_A at the end of the scan to compensate for the intrusion of the cold mirror into the field of view. The 7 colors correspond to the 7 channels as indicated in Table 1. The 85 GHz channels show a saw-tooth pattern presumably due to a small mismatch in the integration timing.

Table 1. Color coding for figures displaying 7 channels or 6 SSM/I.

black	red	green	blue	magenta	cyan	orange
19V	19H	22V	37V	37H	85V	85H
F08	F10	F11	F13	F14	F15	

Table 2. Color coding for figures displaying the 11 inter-satellite overlap periods.

black	red	green	blue	magenta	cyan	orange	black	red	green	blue
F08	F08	F10	F10	F10	F11	F11	F11	F13	F13	F14
F10	F11	F11	F13	F14	F13	F14	F15	F14	F15	F15

4. Inter-Satellite Calibration

4.1. Observed T_A Differences among the 6 SSM/I

The next step in the calibration procedure is to inter-calibrate the 6 SSM/I. To do this, we first make global maps of T''_{Aij} for each SSM/I. The T_A maps represent a 5-day (pentad) average of SSM/I observations within a 1^o latitude/longitude cell. Separate maps are made for observations taken during the morning portion of the orbit and the evening portion. For these maps, T_A is normalized to an incidence angle of 53.25^o, wind direction effects are removed, and the along-scan correction is applied (i.e., we use the double-prime T_A).

Inter-satellite differences are then computed. Table 2 shows the various combinations of satellite overlaps. There are a total of 11 types of overlaps. For each type of overlap, the difference of the satellite-2 T''_{Aij} minus the satellite-1 T''_{Aij} is found. These inter-satellite T_A differences are only found if for a given pentad both satellites have observed the same latitude/longitude cell during the same portion of the orbit (i.e. evening or morning). Figure 2 shows the inter-satellite T_A differences averaged over latitude and longitude for the evening case. Figure 3 show analogous results from the morning case. The 11 different satellite overlap cases are shown by a different color, as indicated in Table 2. (Colors can be reused for the later overlap cases because they are separate for the earlier cases.) Our inter-calibration analysis for Version 6 was done in 2006, thus there are no inter-comparisons after this mid-2006. For the lower frequency channels (19-37 GHz) the inter-satellite T_A differences for the most part lie between -1 K and +1 K. However at 85 GHz, larger differences can be seen.

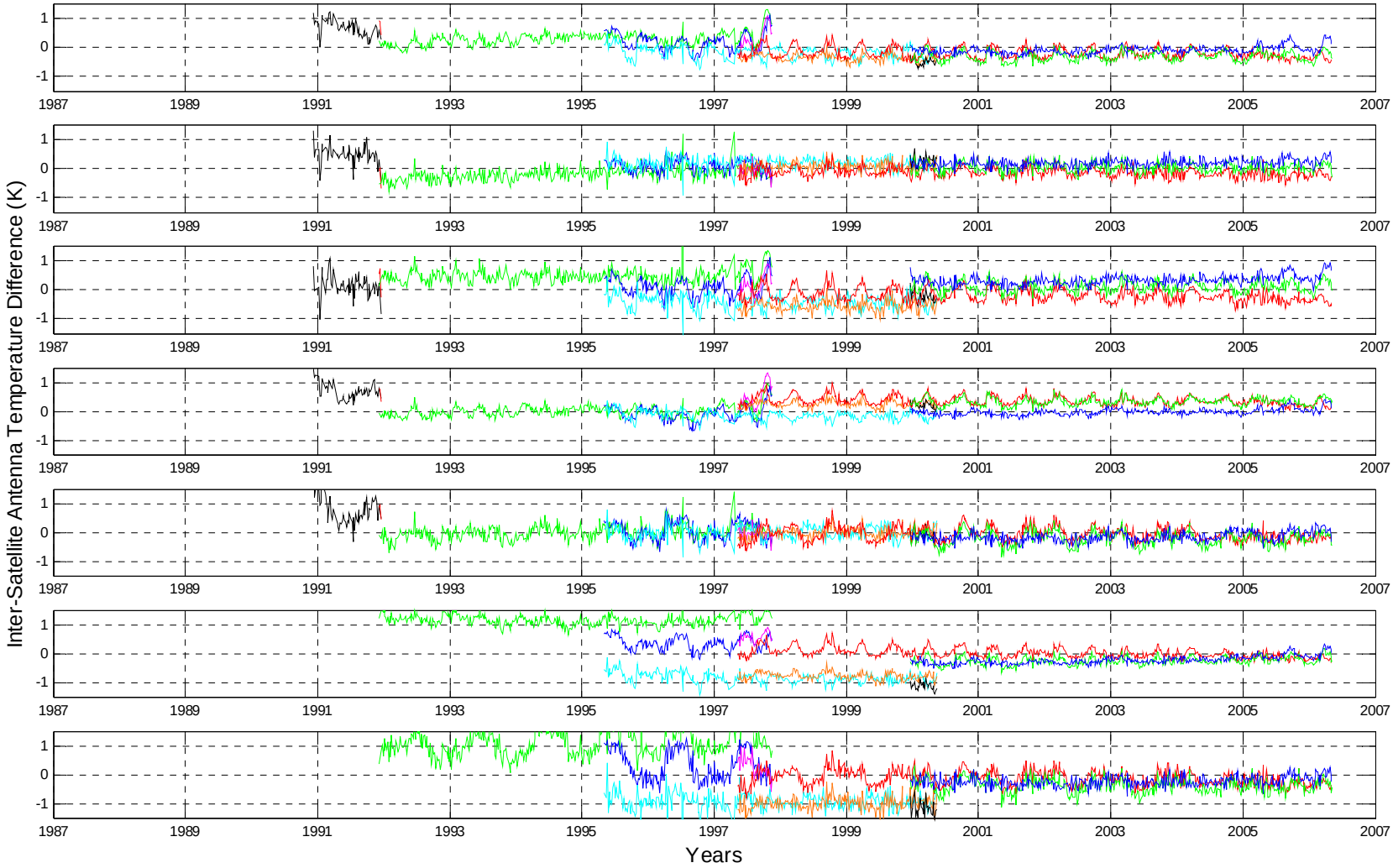

Figure 2. The SSM/I T_A differences for 11 overlap periods. Each overlap period is shown in a different color with the color coding given by Table 2. The 7 frames show the 7 channels going from 19V at the top to 85H at the bottom in the order indicated in Table 1. These results are for the evening portion of the orbit.

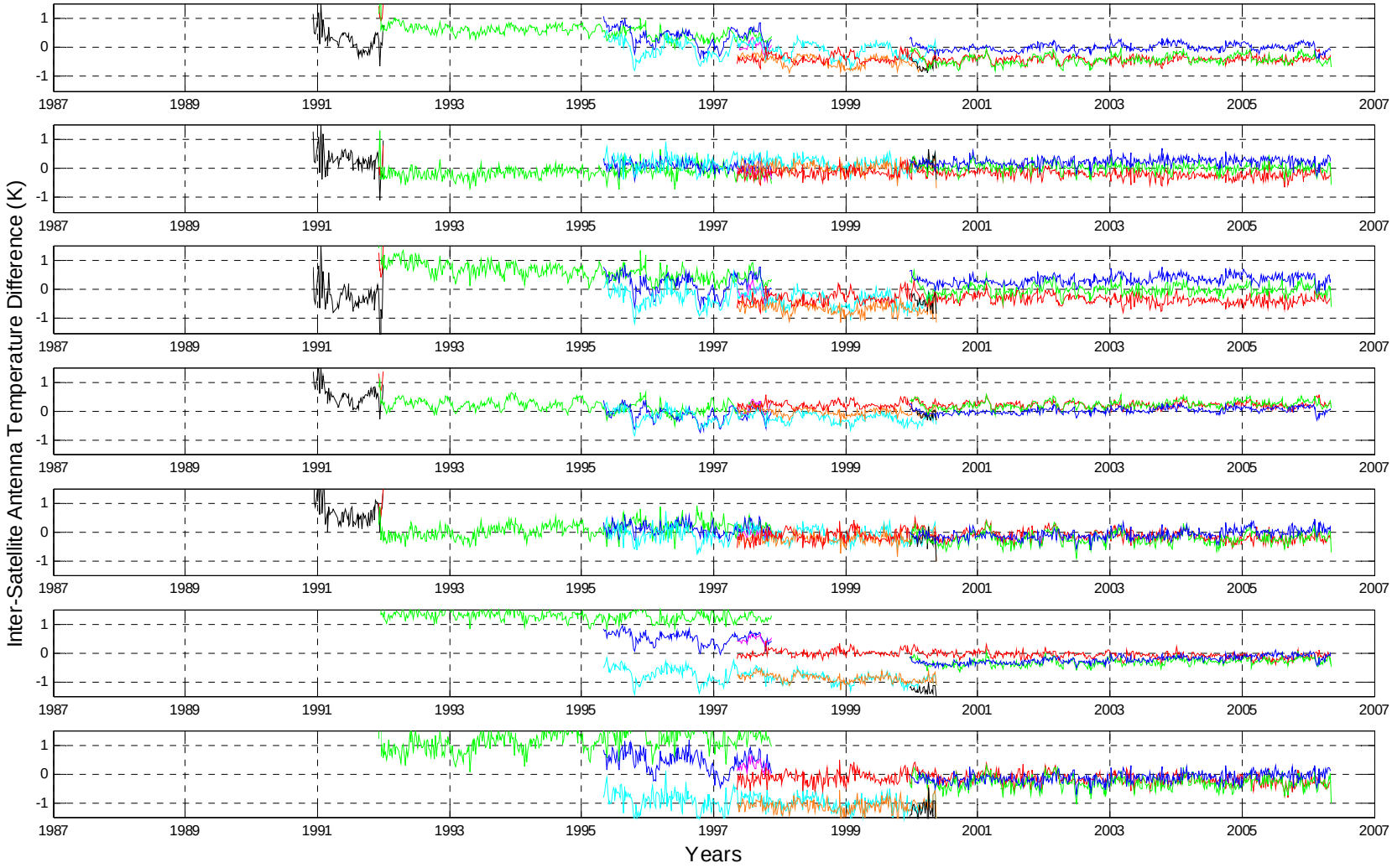

Figure 3. Same as Figure 2 except these results are for the morning portion of the orbit.

4.2. Error Model for Inter-Satellite T_A Differences

Much time was spent analyzing the results in Figure 2 and 3. In addition to averaging over all latitudes for the morning and evening cases, we also reviewed zonal results for which the T_A differences are stratified according to 3 latitude zones: south of 20S, 20S-20N, and north of 20N. Our objective is to find an error model as simple as possible that will explain the inter-satellite T_A differences. After considerable trial and error analyses, we selected the following error model:

$$\Delta T_{Aij} = A_{ij}(\varphi) + B_{ij}(\varphi)\cos\left(\frac{2\pi t}{t_{year}}\right) + C_{ij}(t) + \alpha_{ij}\left(\overline{T}_h - \left\langle \overline{T}_h \right\rangle_j\right) \pm \left[\beta_i (t - t_0) - \frac{1}{2}\eta_i\right] \tag{8}$$

where ΔT_{Aij} is to be subtracted from T''_{Aij} to obtain the desired calibrated T_A. We will now explain each term in equation (8).

The function $A_{ij}(\varphi)$ is called the inter-satellite zonal offset with the angle φ specifying the position of the satellite in its orbit; φ equals 0^o at the satellite's south-most position, 90^o at the equatorial ascending node, and so on. $A_{ij}(\varphi)$ expresses the T_A difference that is found among the 6 SSM/I. To establish an absolute channel level, we required the following:

$$\sum_{j=3}^{6}\sum_{\varphi} A_{ij}(\varphi) = 0 \tag{9}$$

which is requiring $A_{ij}(\varphi)$ be zero when averaged over the 4 later SSM/Is and over φ. This requirement has the effect of establishing an absolute T_A calibration reference that is consistent with the average unadjusted T_A calibration for F11 through F15. The SSM/I on F13 is used as the reference for the φ variation by requiring $A_{i4}(\varphi)$ to be a constant value independent of φ.

Figure 4 shows $A_{ij}(\varphi)$. For most cases, the inter-satellite offsets are nearly constant over the orbit (± 0.2 K), but for certain satellites and certain channels the intra-orbit variation can be significant. For this reason, the inter-satellite offset is modeled as a function of the satellite position angle φ.

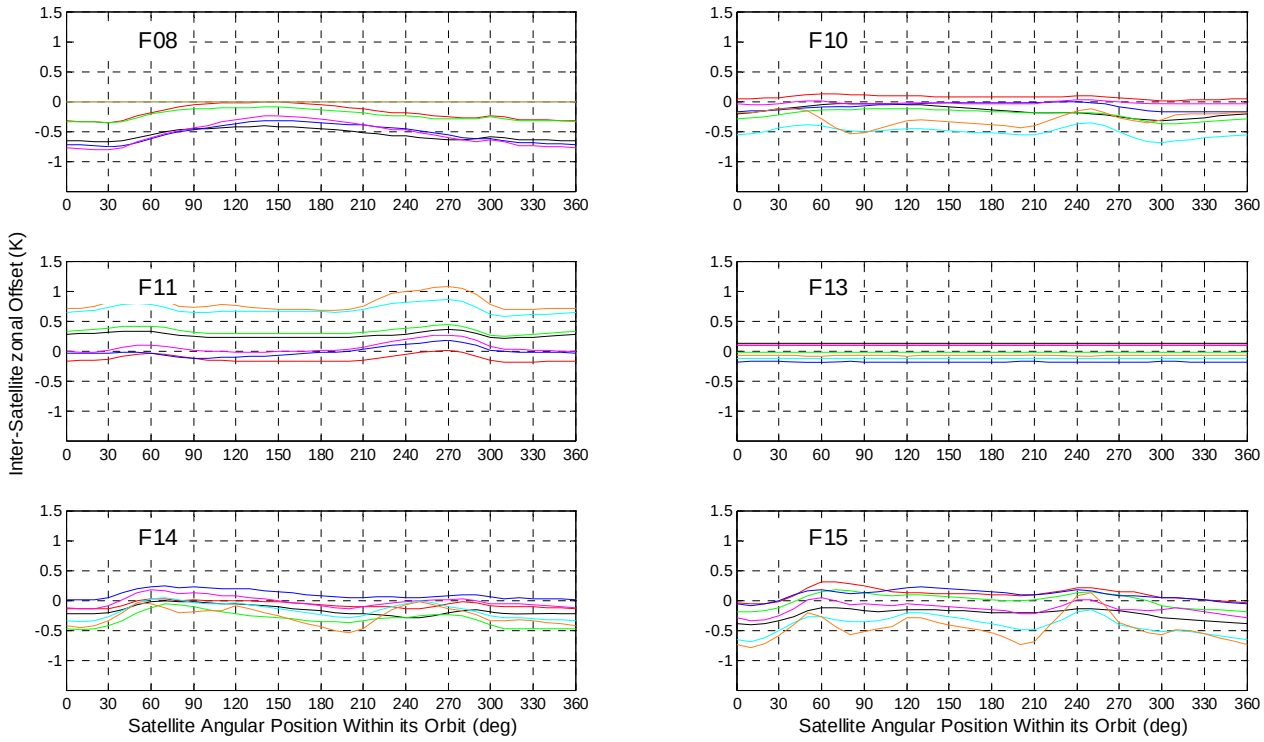

Figure 4. The inter-satellite zonal offset $A_{ij}(\varphi)$ plotted versus satellite position angle φ. The colors denote the 7 SSM/I channels as indicated in Table 1.

The function $B_{ij}(\varphi)$ is a very small term (< 0.1 K), except for F10. It models the seasonal variation of the inter-satellite offset and is only included because comparisons of the F10 SSM/I to the other SSM/I (particularly the 85H channel) showed this term is important for F10. The seasonal variation is specified by the cosine term where t is the time for the observation (hours), and t_{year} is the length of the solar year. $B_{ij}(\varphi)$ for F08 and F13 are set to 0. For F13, F14, and F15, $B_{ij}(\varphi)$ is assumed to be constant (i.e., no variation with φ) and never exceeds 0.07K for these 3 satellites. Figure 5 shows $B_{ij}(\varphi)$.

Function $C_{ij}(t)$ models slow time variations in the inter-satellite offsets. Only 3 SSM/I have this term: F10, F11, and F13. For the other SSM/I, $C_{ij}(t)$ is zero. Figure 6 shows $C_{ij}(t)$ for F10, F11, and F13. Treating the F11 SSM/I are a reference, we saw obvious slow time variations of the F10 T_A relative to F11. The F13 T_A relative to F11 also shows a slow time variation but only during the first year of F13 operation. During the last four years of the F11-F13 over-

lap, the T_A difference shows no obvious variation with time. Because the SSM/I F10 exhibits relatively large calibration errors in many respects, presumably due to it anomalous orbit, we assign the observed F10-F11 time-varying error to F10, with one exception. The F11-F10 T_A difference for 37H shows a very slow monotonic increase going from about -0.2K in 1992 to +0.1K in 1999. As it turns out, a completely separate analysis looking at histograms of wind speed retrievals from F11 shows a slight shift of the left edge of the histograms (i.e., the position of the histogram for wind=0) over the life of F11. The shift was in the positive direction and very closely mimics the observed F11-F10 T_A difference at 37H, which is the primary wind speed channel. So we decided to assign this small component of the time variation to F11. Otherwise F11 seemed very stable, and we assume the remaining part of the time variation is due to problems with F10.

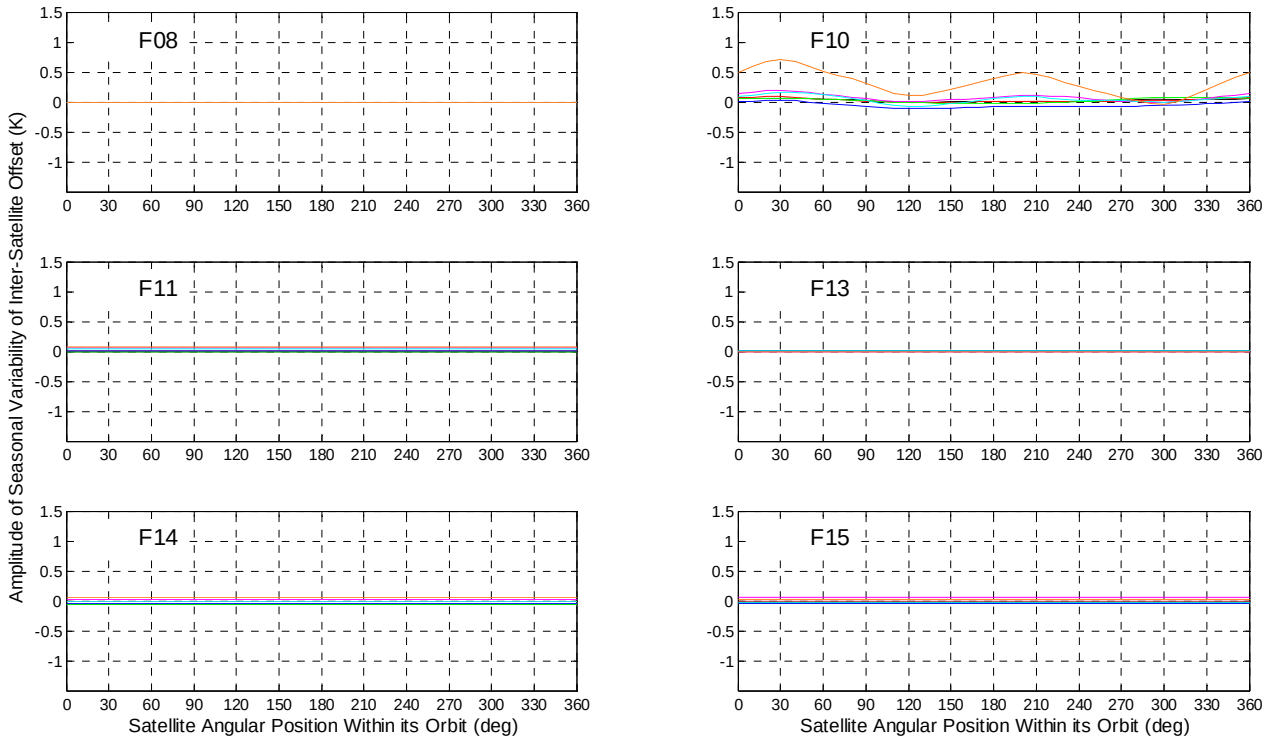

Figure 5. The amplitude of seasonal variability of inter-satellite offset $B_{ij}(\varphi)$ plotted versus satellite position angle φ. The colors denote the 7 SSM/I channels as indicated in Table 1.

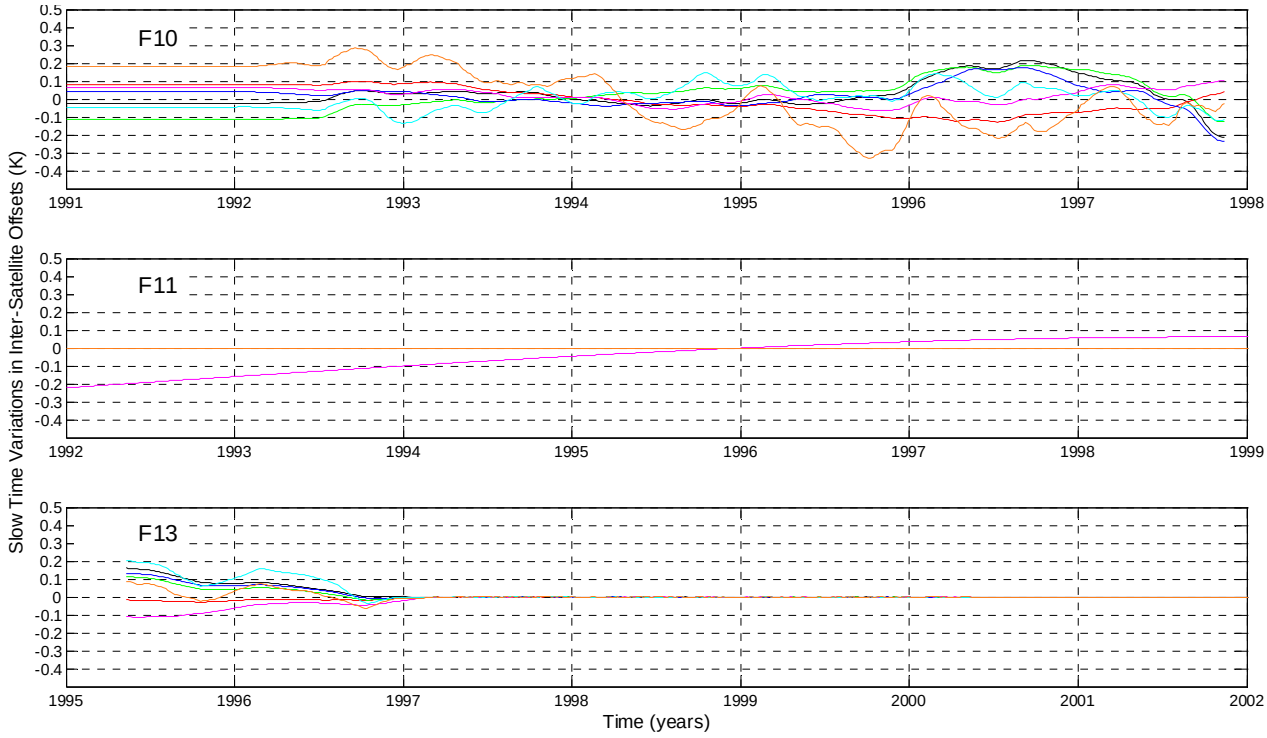

Figure 6. Slow time variations $C_{ij}(t)$ in the inter-satellite offsets. Only 3 SSM/Is (F10, F11, and F13) showed relative time drifts. Colors denote the 7 SSM/I channels as indicated in Table 1.

The F13-F11 T_A differences are harder to explain. In general, F13 seems to be stable and well calibrated. During most of the F11 and F13 overlap period, the two SSM/I track each other very well. It is just the first year after launch that the F13-F11 T_A differences show a slow time variation. It does not have the signature of a diurnal feature. We elected to assign the problem to F13 assuming it was some sort of early mission stabilization. The size of the correction is small being 0.1-0.2 K as is shown in Figure 6.

The α-term in equation (8) is based on our satellite calibration work done for the Microwave Sounding Unit (MSU). The term $\overline{T}_h$ is the hot load temperature defined in Section 2, and $\langle \overline{T}_h \rangle_j$ is the mission-averaged value of $\overline{T}_h$. The MSU and the Advanced MSU (AMSU) are atmospheric profilers that measure air temperature in different layers of the atmosphere. Much work has gone into doing inter-satellite calibration for the series of MSU/AMSU that starts in 1979. One finding from the MSU investigations is that inter-satellite offsets are correlated with the hot-load temperature [*Christy et al*., 2000; *Mears et al*., 2003]. It is not clear why such a correlation exists, but possibly it is related to non-linearities in the radiometer response function. We include

this term, which is called the 'target factor', in our SSM/I error model to see if it could explain some of the observed inter-satellite T_A variation. Table 3 gives the values for $\langle \overline{T}_h \rangle_j$ and α_{ij}. For the MSU analyses [*Mears et al*., 2003], several sensors had α values of 3%. However, for SSM/I the largest α value is 1% for the F15 85V channels, and for the most part α is well below the 1% level. This suggests the target-factor effect is not as serious of a problem for SSM/I as it is for MSU. There were so many other problems with the F10 SSM/I, we did not attempt to compute a target factor, and α is set to 0 for F10.

Table 3. The mission-average hot-load temperature and the target factor *α*.

	F08	F10	F11	F13	F14	F15
$\langle \overline{T}_h \rangle_j$ (K)	264.1232	307.5306	278.0409	291.4749	304.4429	301.4340
19V α	-0.0029	0	-0.0037	0.0046	0.0008	0.0041
19H α	0.0021	0	-0.0013	0.0030	0.0009	0.0016
22V α	-0.0003	0	-0.0002	0.0053	0.0024	0.0056
37V α	-0.0080	0	0.0007	0.0042	0.0009	0.0065
37H α	-0.0088	0	0.0012	0.0076	0.0066	0.0063
85V α	0	0	-0.0001	0.0025	0.0044	0.0106
85H α	0	0	0.0010	0.0048	0.0053	0.0078

The last term is equation (8) is intended to remove natural diurnal variability. The SSM/I views the earth in the early-to-mid morning (5:30 am to 10:00 am) and in the evening (5:30 pm to 10:00 pm). The major contributor to the diurnal signal seen during these periods is clouds, which are drying off in the morning and moistening in the evening. An analysis of the TRMM microwave radiometer observations, which views the Earth through the entire diurnal cycle, indicates that to first order, the change in the antenna temperature can be modeled as a linear decrease in the morning and a linear increase in the evening, with the magnitude of the slope being the same. This slope (K/hour) is denoted by β_i in (8). The plus sign for this term is for morning observations and the minus sign is for evening observations. The time t_0=70200 is the typical time for the evening equator crossing (i.e., 7:30 pm).

The other term η_i in the diurnal model is the typical T_A difference at 7:30 am minus 7:30 pm. To find this term, we first normalize the observations from all the SSM/Is to 7:30 am and 7:30 pm using the β_i term. Then we find a change in water vapor V and liquid cloud water L that best explains the observed 7:30 am minus 7:30 pm difference in T_A. The values found are -0.2 mm and + 0.005 mm for vapor and cloud, respectively. Using typical global values for the derivatives $\partial T_A/\partial V$ and $\partial T_A/\partial L$, a fixed value for η_i is found for each channel. Table 4 gives the values for β_i and η_i. Note when finding inter-satellite T_A differences, the η_i term cancels out.

Table 4. Coefficients describing the diurnal variation in T_A.

	19V	19H	22V	37V	37H	85V	85H
β (K/hour)	0.049	0.080	0.029	0.101	0.197	0.091	0.238
η (K)	0.02	0.04	-0.07	0.21	0.41	0.21	0.57

4.3. Derivation of Coefficients in Error Model

The first step in deriving the coefficients in the error model is to perform a least squares minimization for the 6 overlap periods for F11 through F15 (see Table 2). The quantity that is minimized is the inter-satellite difference. For example for the F13-F11 overlap, the $T''_{Ai4} - T''_{Ai3}$ is minimized. All 6 overlaps are done simultaneously and there are 153 coefficients found for each channel. For each satellite there are 36 coefficients for $A_{ij}(\varphi)$, one for α_{ij}, and one for B_{ij}. ($A_{ij}(\varphi)$ is specified at 10^o increments and for these 4 satellites B_{ij} is assumed independent of φ.) These 38 coefficients times 4 satellites gives a total of 152. There is one additional coefficient β_i that is the same for all satellites. During the minimization, we apply the constraint specified by equation (9), the constraint $B_{i5}(\varphi)$=0, and reasonable smoothing to constrain on the 36 elements of $A_{ij}(\varphi)$. After finding the 153 coefficients and applying the correction to the T_A, the final step in calibrating F11 through F15 is to find the slowly varying time function $C_{ij}(t)$ for F11 and F13. This is done by simply taking the time series of the inter-satellite differences, assigning a difference to a particular satellite as discussed above, and apply appropriate smoothing.

Once the F11 through F15 SSM/I have been fully calibrated, we calibrate F10 keeping the F11 through F15 calibration fixed. The last 1.5 years of F10 is excluded because of problems

that begin to develop with F10. Our major objective is to obtain a good calibration for F10 during the earlier part of its mission so that we can use it to connect F08 with F11. Hence we thought it best to exclude the last part of F10 from the derivation of the calibration coefficients.

For F10, we use the same type of least-squares minimization. In this case there are 3 types of overlaps (F11, F13, F14) and number of coefficients found is 72: 36 for $A_{i2}(\varphi)$ and 36 for $B_{i2}(\varphi)$ (α_{i2} is set to 0 as discussed above). After finding the 72 coefficients and applying the correction to T_A, we find $C_{i2}(t)$ by using F11 as a reference. For the time period before F11, $C_{i2}(t)$ is set to a constant value equal to its value during the early part of the F10-F11 overlap.

The last step is to calibrate F08 for which there are two overlaps: one with F10 and a brief overlap with F11. For F08, $B_{i1}(\varphi)$ is constrained to be zero, and 37 coefficients are found: 36 for $A_{i1}(\varphi)$ and one for α_{i1}. This completes the derivation of the coefficients in the error model. The error model is then subtracted from T''_{Aij} to obtain the fully corrected (triple-prime) T_A:

$$T'''_{Aij} = T''_{Aij} - \Delta T_{Aij} \tag{10}$$

5. Correction to the Earth Incidence Angle

Except for the diurnal term, the error model given by (8) is similar for the evening portion (pm) of the orbit and the morning portion (am). For most channels and satellites the dependence of the offset on the satellite position angle φ is small. Also the am-pm α target factor is similar (and small). Most of the contribution of the target factor is due to the seasonal variability of the hot load temperature. For a given day, the am versus pm difference of the hot load temperature is relatively small. Thus a good approximation for the am minus pm T_A difference is

$$\Delta T_{Aij,am} - \Delta T_{Aij,pm} \approx 2\beta_i (t - t_0) - \delta_i \tag{11}$$

where just the diurnal term remains. The diurnal variation is mostly due to the atmosphere which is evidence in Table 4 by the fact that at 37 GHz the h-pol term is twice the v-pol. A well-known method to remove the atmospheric influence from radiometer measurements is to use the following linear combination of polarizations:

$$T_{Ax} = T_{A37h} - 2T_{A37v} \tag{12}$$

where we have introduce the subscript *x*, which replaces the channel subscript *i*, and denotes what we call the 'x-polarization'. Using this polarization in (11) gives

$$\Delta T_{Axj,am} - \Delta T_{Axj,pm} \approx 2\beta_x \left(t - t_0\right) - \delta_x \tag{13}$$

and Table 4 shows that the value for β_x and η_x is very small.

We thus expect the am-pm difference of T'''_{Axj} to be very small if our error model is sufficient. The triple-prime T_A supposedly has all calibration problems removed and using x-pol should eliminate diurnal features. However, when am-pm T'''_{Axj} is plotted versus time, we see obvious oscillations with fixed periodicities, particularly for F10. We think the most likely explanation for these features is an error in specifying θ_{eia}. The SSM/I flies on a Defense Meteorological Satellite Program (DMSP) spacecraft. Our knowledge of the DMSP spacecraft is limited, but we think the attitude control system is based on a horizon sensor. There is no attitude information given with the SSM/I science on ephemeris data. We have no values of roll, pitch, or yaw to reference. Supposedly, the DMSP spacecraft flies a geodetic mission with the horizon sensor keeping the spacecraft nadir pointing perpendicular to the Earth's geoid. Given no attitude information, we must simply assume geodetic geometry when computing θ_{eia}. Some error between our assumed geodetic θ_{eia} and the true θ_{eia} is to be expected, particularly for the F10 DMSP which was in an anomalous orbit with a relatively high eccentricity due to a partial launch failure.

The x-pol is very sensitive to incidence angle. A 1^o change in θ_{eia} produces about a -4 K change in T_{Ax}. We transform the time oscillations in T'''_{Axj} to time oscillation in θ_{eia} using a typical $\partial T_{Ax} / \partial \theta_{eia}$ derivative value of -4.23 K/deg. The resulting incidence angle error $\Delta\theta_{eia}$ is then modeled as

$$\Delta\theta_{eia,j} = D_j\left(t\right)\sin\varphi \tag{14}$$

where $D_j\left(t\right)$ is a slowly varying function of time. This model is the simplest that would produce the observed am-pm differences in T'''_{Axj}. Figure 7 shows $D_j\left(t\right)$ for each of the 6 SSM/I. The oscillations with fixed periodicities discussed above are clearly evident. $\Delta\theta_{eia,j}$ is to be subtracted from the geodetic θ_{eia}.

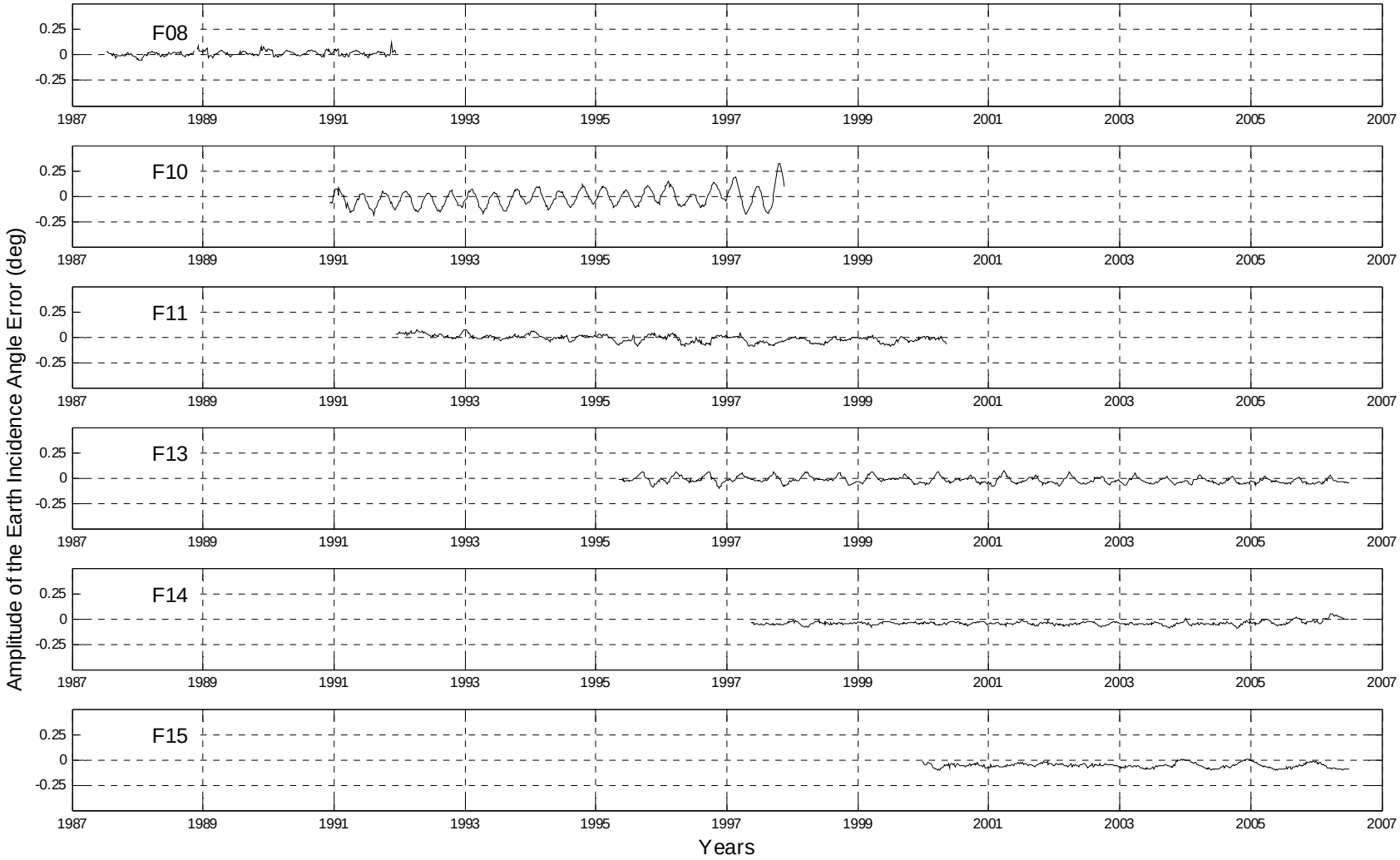

Figure 7. Amplitude $D_j(t)$ of the Earth incidence angle error for each SSM/I.

We note that the x-pol T_A is also sensitive to wind speed variations. However, it is difficult to imagine diurnal features in wind speed that would be large enough and would have the periodicities that we are seeing in Figure 7. Incidence angle error is a much more likely cause.

6. A Small Final Adjustment to the F10 T_A

The oscillation in Figure 7 exhibited by F10 has a fixed period of 122 days, which is the same period exhibited by the orbit's angle of perigee and eccentricity (see Figure 4 in *Wentz* [1991]). As a final (and very minor) measure after applying all the corrections discussed above including the correction to θ_{eia}, we do a harmonic analysis just for F10 to see if there is any residual error correlated with a 122-day period. The harmonic analysis is based on the T_A difference of F10 relative to F11. The following residual was found:

$$\Delta T_{Ai,122} = G_{1i} \sin\varphi \sin\frac{2\pi t}{t_{122}} + G_{2i} \cos\varphi \cos\frac{2\pi t}{t_{122}} \tag{15}$$

where t_{122} is 122 days in terms of hours. The G coefficients are given in Table 5 and none exceed 0.2 K. $\Delta T_{Ai,122}$ is subtracted from T'''_{Ai2} as a final correction to F10. To avoid adding a fourth prime to T_A, we redefine the triple-prime T_A to include this final little adjustment.

Table 5. Coefficients for residual F10 T_A error with the 122-day period

	19V	19H	22V	37V	37H	85V	85H
G_1 (K)	0.09	0.02	0.02	0.03	0.07	0.06	0.07
G_2 (K)	0.13	-0.03	0.16	0.18	-0.05	0.02	-0.04

7. Fully Corrected Antenna Temperatures

Inter-satellite T_A differences for the fully corrected T'''_{Aij} are then computed for the 11 overlaps periods. The procedure is the same as described in Section 4.1. Figures 8 (evening) and 9 (morning) show the results. As compared to Figures 2 and 3, the inter-satellite T_A differences are greatly reduced. Note that when normalizing the T_A to an incidence angle of 53.25^0 as prescribed by equation (3), the corrected incidence angle is now used.

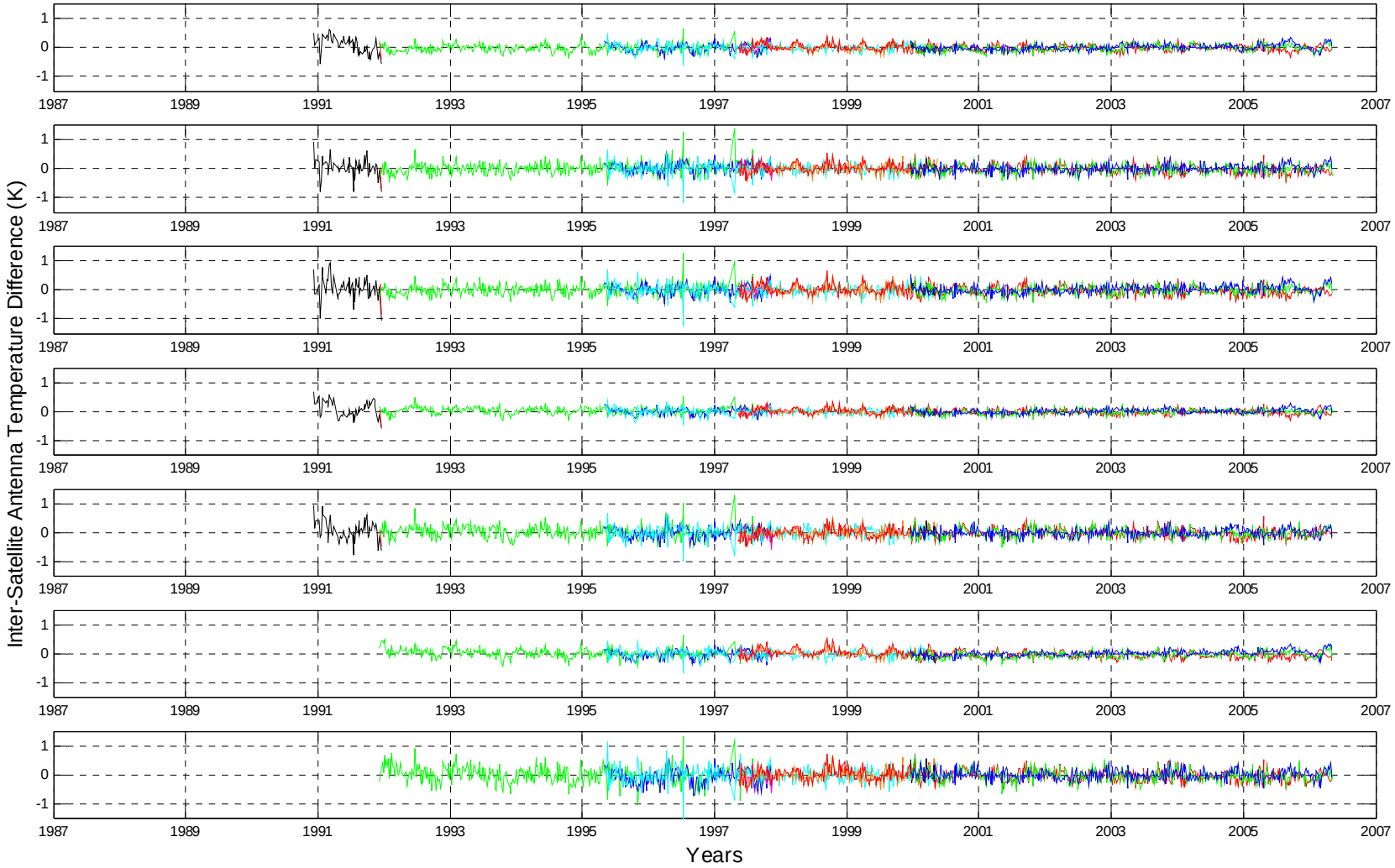

Figure 8. SSM/I T_A differences for 11 overlap periods after applying all the corrections. Each overlap period is shown in a different color with the color coding given by Table 2. The 7 frames show the 7 channels going from 19V at the top to 85H at the bottom in the order indicated in Table 1. These results are for the evening portion of the orbit.

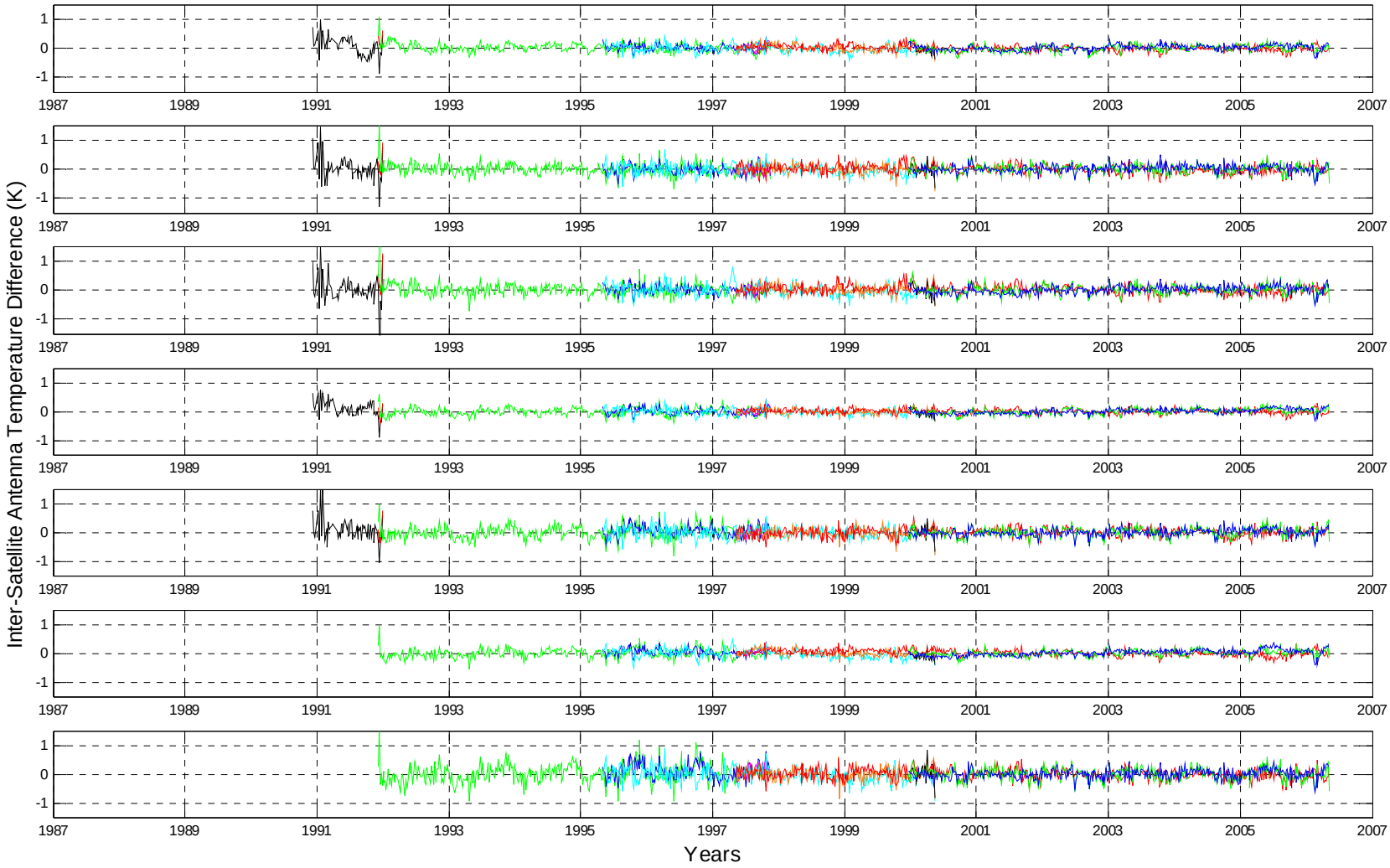

Figure 9. Same as Fig. 8 except these results are for the morning portion of the orbit.

8. Comparison of Morning and Evening T_A

It is also informative to look at the morning minus evening T_A difference for a given SSM/I. As mentioned above the T_A maps are partitioned into the evening portion (pm) of the orbit and the morning portion (am). Am-pm T_A differences are found but only if for a given pentad there is an observation of the same latitude/longitude cell for both the morning and evening. These T_A difference are then averaged over all latitudes and longitudes and plotted versus time. Figure 10 show the results for T''_{Aij}, which is the T_A before applying the corrections (8), (14), and (15). The most obvious features are the oscillations in incidence angle error for F10 and to a lesser extent for F13. Figure 11 is the same as Figure 10 except all corrections have been applied. There are still some unexplained features, but the major oscillations have been removed.

9. RADCAL Beacon Correction for F15

On 14 August 2006, a radar calibration (RADCAL) beacon was activated on F15. This radar interfered with the SSM/I, primarily the 22V channel. We apply a correction to the F15 22V channel to mitigate the RADCAL interference [*Hilburn and Wentz*, 2008; *Hilburn* 2009]. This correction is given by

$$\Delta T_{A,radcal} = H(\omega)\,\Gamma\left(\overline{T}_h\right) \tag{16a}$$

$$\Gamma\left(\overline{T}_h\right) = c_0 + c_1\overline{T}_h + c_2\overline{T}_h^2 \tag{16b}$$

where $\Delta T_{A,radcal}$ is to be subtracted from the T_A measurement. The term $H(\omega)$ is a table of 64 values corresponding to the SSM/I scan position and is shown in Figure 12. The coefficients c_0, c_1, and c_2 are 79.8977, -0.518557 K^{-1}, and 8.51691e-4 K^{-2}, respectively. At the extremes, if $\Gamma\left(\overline{T}_h\right)$ falls below 1, it is set to 1; if it exceeds 3.5, it is set to 3.5. This correction is applied starting with F15 orbit 34478.

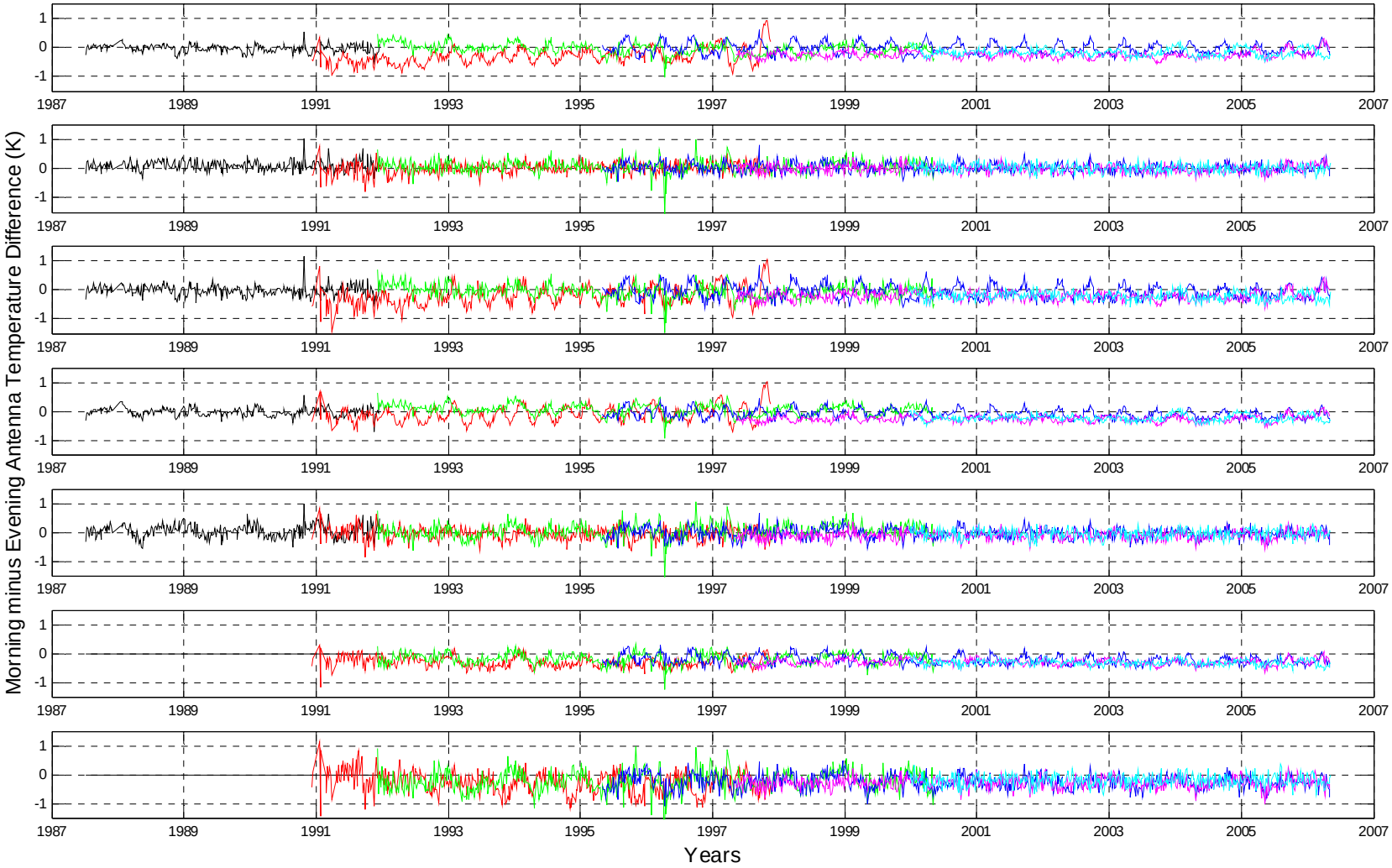

Figure 10. The am minus pm T_A differences for the 6 SSM/I. Each SSM/I is shown in a different color with the color coding given by Table 1. The 7 frames show the 7 channels going from 19V at the top to 85H at the bottom in the order indicated in Table 1. These results are before applying the T_A and incidence angle corrections.

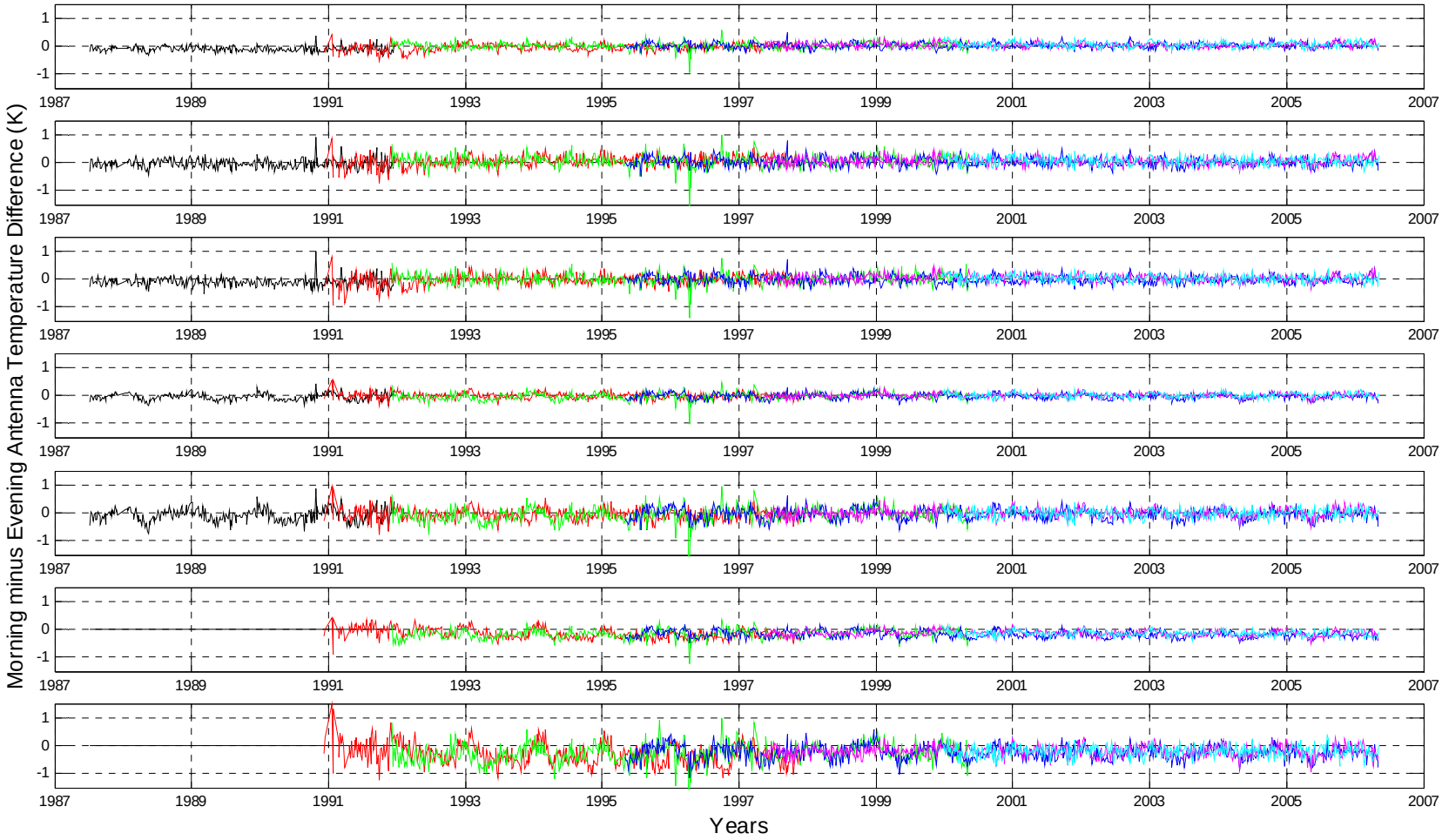

Figure 11. Same as Fig. 10 except the T_A and incidence angle corrections have been applied.

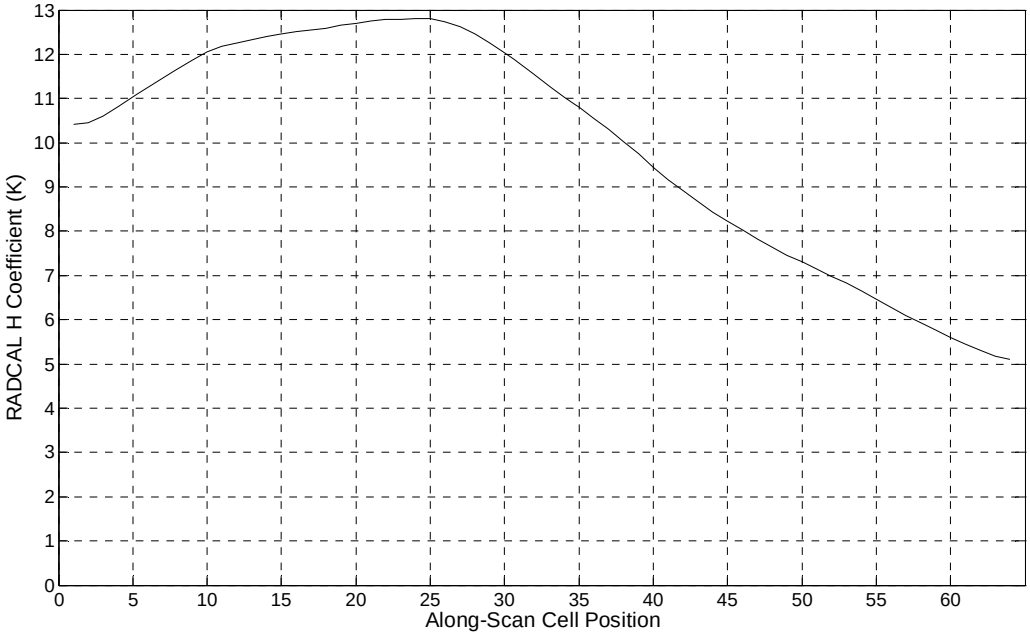

Figure 12. The RADCAL $H(\omega)$ coefficient plotted versus scan position.

10. Version 6 Mean Channel Level Compared to Version 5

After completing the V6 calibration, we compared the overall mean level of each channel (averaged over all satellites and all times) with the previous V5 calibration. We found small offsets of the order of 0.1 K, or less. The V6 minus V5 offsets are shown in Table 6. The principle reason these version offsets occur is that the V5 overall calibration was based on an average of all 6 SSM/I, whereas the V6 overall calibration is based on just the last 4 SSM/I, as prescribed by equation (9). The V6 calibration is much more extensive than that done for V5 and represents a major step forward, particularly with regards to inter-calibrating the 6 SSM/I. However, there are reasons for not changing the overall absolute level of the 7 channels. The main reason is that V5 datasets were in wide use, and the users did not want a change in the absolute level. So the V6-V5 channel offsets are subtracted from the T_A to bring V6 into alignment with V5. Note that the same channel offsets are added to all 6 SSM/I and this adjustment as no effect on relative calibration. With this adjustment, the overall mean channel level is more indicative of the average of all 6 SSM/I. This is a very small adjustment, and Users not wanting to implement this final normalization are free to added back in the values in Table 6.

Table 6. The difference in the overall mean channel level for V6 compared to V5.

Channel	V6-V5 channel offsets (K)
19V	-0.11
19H	-0.01
22V	-0.03
37V	-0.12
37H	-0.05
85V	-0.07
85H	0.00

11. Computation of Earth Brightness Temperature

Antenna temperature is a measure of radiant power entering the feedhorn. It is computed by integrating the brightness temperature environment over the gain pattern of the SSM/I parabolic reflector and feedhorn assembly. About ¾ of the surrounding environment consists of cold space at a temperature near 2.7 K and the remaining ¼ is the Earth, which has a brightness temperature T_B between 100 and 300 K, depending on the scene. Thus, the antenna temperature is biased low relative to the Earth T_B. In addition, some Earth scenes are very polarized, particularly the oceans, and the antenna gain pattern tends to mix polarizations. As a result, the antenna temperature is not as polarized at the Earth T_B.

These two effects are commonly characterized by the antenna spillover δ, which is the fraction of power coming from cold space, and the polarization leakage χ, which is the fraction of polarization mixing, and the integration over the field of view is approximated by [*Wentz*, 1991]

$$T_{Ap} \approx \left(1-\delta_p\right)\frac{T_{Bv}+\chi_p T_{Bh}}{1+\chi_p}+\delta_p T_{Bc} \tag{17}$$

where subscript p denotes polarization (either v or h), T_{Bc} is the brightness temperature of cold space, and T_{Bv} and T_{Bh} are the Earth v-pol and h-pol brightness temperatures. The spillover δ and leakage χ can be derived in an optimum way by first defining T_{Bv} and T_{Bh} to represent an average over some prescribed areal extent on the Earth (we use the 3-dB footprint), and then fitting (17) to the antenna temperature coming from the exact integration. This fitting procedure was done for the F08 antenna patterns [*Wentz*, 1991], and the results are shown in Table 7.

Table 7. Antenna spillover and polarization leakage used for all SSM/I

	Spillover, δ	Leakage, χ
19V	0.03199	0.00379
19H	0.03199	0.00525
22V	0.02685	0.00983
37V	0.01434	0.02136
37H	0.01434	0.02664
85V	0.01186	0.01387
85H	0.01186	0.01967

Field antenna pattern measurements were made for each SSM/I. These measured patterns are different for the different SSM/I. However, when we used these separately measured antenna patterns (i.e., different δ,χ for different SSM/I), the inter-satellite offsets became larger. We concluded that most of the difference exhibited by the different set of antenna patterns is due to measurement error, and that in fact the antennas for the 6 SSM/I were more alike that suggested by the field measurements. In view of this, we use the F08 δ,χ values for all SSM/I. The inter-satellite offsets that we do see are probably in part due to the δ,χ values being different for the different sensors, but not as different as suggested by the field measurements.

For 19, 37, and 85 GHz, there are two equations for (17): one for T_{Av} and the other for T_{Ah}, in two unknowns: T_{Bv} and T_{Bh}. These equations are easily inverted to yield T_{Bv} and T_{Bh}. At 22 GHz, there is only v-pol for SSM/I, and the following approximation is used

$$T_{B22v} = 1.01993 T_{A22v} + 1.994 \tag{18}$$

See *Wentz* [1991] for details on the derivation of (18).

12. References

Christy, J. R., R. W. Spencer, et al. (2000). "MSU Tropospheric Temperatures: Dataset Construction and Radiosonde Comparisons." Journal of Atmospheric and Oceanic Technology 17(9): 1153-1170.: MSU Tropospheric Temperatures: Dataset Construction and Radiosonde Comparisons. *Journal of Atmospheric and Oceanic Technology 17*(9): 1153-1170.

Colton, M. C. and G. A. Poe, 1999: Intersensor Calibration of DMSP SSM/I's: F-8 to F-14, 1987-1997. *IEEE Transactions on Geoscience and Remote Sensing, 37*, 418-439.

Hilburn, K. A. and F. J. Wentz, 2008: Mitigating the Impact of RADCAL Beacon Contamination on F15 SSM/I Ocean Retrievals. *Geophysical Research Letters, 35*, L18806, doi:10.1029/2008GL034914.

Hilburn, K. A. and F. J. Wentz, 2008: Intercalibrated Passive Microwave Rain Products From the Unified Microwave Ocean Retrieval Algorithm (UMORA). Journal of Applied Meteorology and Climatology, 47, 778-794.

Hilburn, KA, 2009: Including Temperature Effects in the F15 RADCAL Correction. *RSS Technical Report 051209*, available from Remote Sensing Systems, www.remss.com.

Hollinger,J., R. Lo, G. Poe, R. Savage, and J. Pierce, 1987: Special Sensor Mirowave/Imager User's Guide. *Naval Research Laboratory Report*, Washington DC.

Mears, C. A., M. C. Schabel, and F. J. Wentz, 2003: A Reanalysis of the MSU Channel 2 Tropospheric Temperature Record. *Journal of Climate, 16*, 3650-3664.

Wentz, F. J., 1988: User's Manual SSM/I Antenna Temperature Tapes. *RSS Technical Report 032588*, available from Remote Sensing Systems, Santa Rosa, CA.

Wentz, F. J., 1991: Revision 1 User's Manual SSM/I Antenna Temperature Tapes. *RSS Technical Report 120191*, available on web site:
http://www.remss.com/papers/ssmi/TA/SSMI_TA_manual_rev_1_part_1.pdf,
http://www.remss.com/papers/ssmi/TA/SSMI_TA_manual_rev_1_part_2.pdf

Wentz, F. J., 1992: Measurement of Oceanic Wind Vector Using Satellite Microwave Radiometers. *IEEE Transactions on Geoscience and Remote Sensing, 30*(5), 960-972.

Wentz, F. J., 1993: Revision 2 User's Manual SSM/I Antenna Temperature Tapes. *RSS Technical Report 120193*, available on web site:
http://www.remss.com/papers/ssmi/TA/SSMI_TA_manual_rev_2.pdf

Wentz, F. J., 1997: A Well Calibrated Ocean Algorithm for Special Sensor Microwave / Imager. Journal of Geophysical Research, 102, 8703-8718.

Wentz, F. J. and M. C. Schabel, 2000: Precise Climate Monitoring Using Complementary Satellite Data Sets. Nature, 403, 414-416.

Wentz, F. J., L. Ricciardulli, K. A. Hilburn, and C. A. Mears, 2007: How Much More Rain Will Global Warming Bring? Science, 317, 233-235. Specific information available in the supplementary online material at http://www.sciencemag.org/cgi/data/1140746/DC1/1

13. Appendix A. Software for Applying the Calibration Procedures

The following Fortran subroutine performs the mathematical operations described in the document for doing the inter-satellite calibration and incidence angle correction.

```
c     inputs:

c     isat is ssmi number.  it goes from 1 to 6 and corresponds to f08, f10, f11, f13, f14, f15
c     itime87 is the scan time.  it is in terms of seconds from begin of 1987
c     zang is the satellite position angle in degrees
c     hltemp is the hot load temperature in Kelvin

c     outputs:
c     array ta_offset(7) is the correction to the unadjusted ta.  ta_offset is to be subtracted from the unadjusted ta.
c     the 7 elements correspond to the ssmi 7 channels:  19V, 19H, 22V, 37V, 37H, 85V, 85H
c     thtcor is the correction to the incidence angle.  thtcor is to be subtracted from the geodetic incidence angle

subroutine ssmi_v06_calibration(isat,itime87,zang,hltemp, ta_offset,thtcor)
implicit none

integer(4), parameter :: nsat=6
integer(4), parameter :: nch= 7

integer(4), intent(in)  :: isat,itime87
real(4),    intent(in)  :: zang,hltemp

integer(4) istart,ich,i1,i2,j1,j2

real(4)   cosang,ta_offset(nch),thtcor

c     variables read in from tables
real(4) thotavg(nsat),alpha(nsat,nch),acoef(36,nsat,nch),bcoef(36,nsat,nch)
real(4) ccoef_f13(432,nch),ccoef_f10(432,nch),gcoef1(nch),gcoef2(nch)
real(4) thtcor_tab(2000,nsat)

real(4) dta_v05(nch)
real(4) ang,a1,a2,b1,b2,brief,ccoef,pentad,xyear,sinpent,cospent,sinzang,coszang

data dta_v05/  -0.106,   -0.014,   -0.031,   -0.116,   -0.046,   -0.067,  0.001/
data istart/1/



c     ================================================================================================================
c     ================================= begin of intialization block =================================================
c     ================================================================================================================
```

```
if(istart.eq.1) then
istart=0

open(3,file='o:\ssmi5\v06\calibrate\v6_cal_coefs.dat',status='old',access='sequential',form='binary')
read(3) thotavg  !mission average hot load temperature
read(3) alpha    !target factors
read(3) acoef
read(3) bcoef
read(3) ccoef_f13
read(3) ccoef_f10
read(3) gcoef1
read(3) gcoef2
close(3)

open(3,file='o:\ssmi5\v06\calibrate\v6_eia_correction.dat',status='old',access='sequential',form='binary')
read(3) thtcor_tab
close(3)

endif


c     ================================================================================================================
c     ================================== end of intialization block ==================================================
c     ================================================================================================================

sinzang=sind(zang)
coszang=cosd(zang)

ang=(360.d0*itime87)/(365.25d0*86400.d0)
cosang=cosd(ang)

pentad=0.5 + itime87/438300.d0
sinpent=sind(360.*(pentad/24.1))  !122 day period
cospent=cosd(360.*(pentad/24.1))  !122 day period

if(zang.lt.0 .or. zang.gt.360) stop 'zang oob in fd_ta_adjustment2, pgm stopped'
brief=zang/10.
if(brief.gt.35.999) brief=35.999
j1=1+brief
j2=j1+1
b1=j1-brief
b2=1.-b1
if(j1.eq. 0) j1=36
if(j2.eq.37) j2= 1

ta_offset=
b1*acoef(j1,isat,:)+b2*acoef(j2,isat,:)+(b1*bcoef(j1,isat,:)+b2*bcoef(j2,isat,:))*cosang+alpha(isat,:)*(hltemp-thotavg(isat))

if(isat.eq.3) then
xyear=1987 + itime87/31557600.d0
ccoef= -0.472002 + 0.062637*(xyear-1992) - 0.000454*(xyear-1992)**3 + 0.2505
```

```
ta_offset(5)=ta_offset(5) + ccoef
endif

if(isat.eq.4) then
brief=pentad-577
if(brief.lt.  0.00) brief=  0.00
if(brief.gt.430.99) brief=430.99
i1=1+brief
i2=i1+1
a1=i1-brief
a2=1.-a1
do ich=1,nch
ccoef=a1*ccoef_f13(i1,ich) + a2*ccoef_f13(i2,ich)
ta_offset(ich)=ta_offset(ich) + ccoef
enddo
endif

if(isat.eq.2) then
brief=pentad-361
if(brief.lt.  0.00) brief=  0.00
if(brief.gt.430.99) brief=430.99
i1=1+brief
i2=i1+1
a1=i1-brief
a2=1.-a1
do ich=1,nch
ccoef=a1*ccoef_f10(i1,ich) + a2*ccoef_f10(i2,ich)
ta_offset(ich)=ta_offset(ich) + ccoef        + gcoef1(ich)*sinzang*sinpent + gcoef2(ich)*coszang*cospent
enddo
endif

ta_offset=ta_offset - dta_v05  !normalize to V5 channel levels

brief=pentad-1
i1=1+brief
i2=i1+1
a1=i1-brief
a2=1.-a1
if(i1.lt.1 .or. i2.gt.2000) stop 'error in sat_offsets, pgm stopped'
thtcor=(a1*thtcor_tab(i1,isat) + a2*thtcor_tab(i2,isat))*sinzang

return
end
```

14. Appendix B. Evolution of SSM/I Versions and Validation of Version 6

The generation of the SSM/I T_A datasets has gone through six major improvements (i.e., version changes), starting with Version-1 in 1988 [*Wentz*, 1988]. The primary emphasis of Version-1 was data compression. In the late 1980s and early 1990s, the only access to SSM/I T_A datasets was 6250 bpi tapes stored at NESDIS. There were 4 tapes/day and users were required to pay $175/tape. These large volumes and costs essentially made the SSM/I T_A datasets unavailable to the research community. As part of a Small Business Innovation Research (SBIR) program, RSS developed a technique for compacting the SSM/I T_A (no information lost) onto monthly Exabyte™ tapes. This provided an affordable means for institutions to obtain a complete dataset of SSM/I observations. Nearly all of the SSM/I scientific research during this early phase utilized these "Compact Tapes".

Version-2 implemented a more user-friendly format, more accurate geolocation, and an along-scan correction for the antenna temperatures [*Wentz,* 1991]. Version-3 extended the data set to include the second SSM/I launched in December 1991 [*Wentz,* 1993]. This was the first version to include intersatellite calibration coefficients for matching the F08 and F10 SSM/I sensors.

In 1997, Version-4 was released. At this point four SSM/I sensors had been launched (F08, F10, F11, and F13), and two more would soon go into space. It was becoming apparent that this series of six SSM/I was playing a very important role in climate monitoring. Thus, we did a more careful intersatellite calibration that included diurnal variability and intra-orbit calibration variability. Also, further refinements were made to the SSM/I pointing geometry to achieve better geolocation. Version-4 was the mainstay for several years, being replaced by Version-5 in 2002.

Version-5 was relatively short lived due to subtle calibration problems that caused small spurious trends in the climate retrievals (the SSM/I record had become long enough at this point to detect such errors). The problem was due to subtle correlations in our derivation of the 'target factors' for the F10 and F14 SSM/I. Like the Microwave Sounding Unit (MSU), some of the SSM/I exhibit errors that are correlated with the hot-load target temperatures, and we removed these errors using the "target multiplier" approach [*Mears et al*., 2003]. These problems, along

with their solutions, are discussed in *Wentz et al*. [2007]. Application of the solutions described herein provided the current V6 SSM/I T_A and T_B dataset.

The primary validation of the V6 T_A and T_B datasets is through their resulting geophysical retrievals. For example, one of the most critical requirements for an CDR dataset is that it be free of spurious long-term trends. Validation of this requirement can be obtained by analyses of the resulting geophysical retrievals. Comparison of the wind speeds retrieved from the V6 T_B with buoys and scatterometers indicates a trend error of 0.05 m/s/decade at the 95% confidence level over the 1987 to 2006 time period [*Wentz et al*., 2007]. The standard error on the water vapor trend (1987-2006) is 0.2% per decade [*Wentz and Schabel*, 2000]. With respect to precipitation, when diurnal effects are removed, the agreement among different SSM/I is 3% [*Hilburn and Wentz*, 2008b]. Note that some of this 3% difference is probably due to residual geophysical effects such as 'beamfilling' rather than T_B intercalibration error. Still, 3% is the best inter-sensor precipitation agreement yet achieved from any SSM/I T_B dataset.

Further validation is obtained from our users. Our SSM/I V6 T_A and T_B datasets are in use at about 20 institutions including the National Snow and Ice Data Center (NSIDC), the NASA Goddard Global Modeling and Assimilation Office (GMAO), Global Precipitation Climatology Project (GPCP), EUMETSAT, Max-Plank Institute for Meteorology, and the Remote Sensing Technology Center of Japan. The V6 geophysical products (wind/vapor/cloud/rain/ice) are freely available on the web through the sponsorship of NASA's REASoN and MEaSUREs programs. Approximately 40 users consistently download the RSS V6 geophysical products on a daily-to-weekly basis in addition to about 4000 occasional users. The feedback we receive from this broad user community has helped to identify problems in the past and provides us with more confidence that the V6 SSM/I V6 T_A and T_B datasets represent a highly accurate climate data record.